Development of a turbulence model based on recursion renormalization group theory

Ye Zhou
Institute for Computer Applications in Science and Engineering, NASA Langley Research Center, Hampton, Virginia 23681

George Vahala
College of William and Mary, Williamsburg, Virginia 23185

S. Thangam
Stevens Institute of Technology, Hoboken, New Jersey 07030

(Received 21 July 1993; revised manuscript received 22 November 1993)

An anisotropic turbulence model for the local interaction part of the Reynolds stresses is developed using the recursion renormalization group theory (r-RNG)—an interaction contribution that has been omitted in all previous Reynolds stress RNG calculations. The local interactions arise from the nonzero wave number range, $0<k<k_c$, where k_c is the wave number separating the subgrid from resolvable scales while the nonlocal interactions arise in the $k\rightarrow 0$ limit. From ϵ-RNG, which can only treat nonlocal interactions, it has been shown that the nonlocal contributions to the Reynolds stress give rise to terms that are quadratic in the mean strain rate. Based on comparisons of nonlocal contributions to the eddy viscosity and Prandtl number from r-RNG and ϵ-RNG theories (ϵ is a small parameter), it is assumed that the nonlocal contribution to the Reynolds stress will also be very similar. It is shown here, by r-RNG, that the local interaction effects give rise to significant higher-order dispersive effects. The importance of these new terms for separated flows is investigated by considering turbulent flow past a backward facing step. On incorporating this r-RNG model for the Reynolds stress into the conventional transport models for turbulent kinetic energy and dissipation, it is found that very good predictions for the turbulent separated flow past a backward facing step are obtained. The r-RNG model performance is also compared with that of the standard K-ε model (K is the kinetic energy of the turbulence and ε is the turbulence dissipation), the ϵ-RNG model, and other two-equation models for this back step problem to demonstrate the importance of the local interactions.

PACS number(s): 47.27.Lx, 47.60.+i, 47.27.Qb

I. INTRODUCTION

Turbulent flows of scientific and engineering importance are characterized by a broad spectrum of length and time scales. While the physical aspects of turbulent flows are best described by the equations of motion, limitations in computer capacity and speed preclude their direct solution for complex flows of relevance to technical applications. The current practice for high Reynolds number flows of practical interest therefore involves some type of modeling for Reynolds stresses. The commonly used turbulence models are based on the calculation of one-point first and second moments such as the mean velocity, mean pressure, and turbulent kinetic energy. Among these, the two-equation turbulence models that involve the use of transport equations for the turbulent field parameters that involve the length and the time scales are probably the most widely used. They involve the simplest level of Reynolds stress closure that do not depend specifically on the flow geometry. (For an excellent review of recent trends in analytical methods for Reynolds stress closure, the reader is referred to Speziale [1].)

In its standard form the two-equation Reynolds stress turbulence models involve the turbulence kinetic energy and dissipation based on a Boussinesq-type approximation [2] of the form

$$\tau_{ij}=-\tfrac{2}{3}K\delta_{ij}+\nu_T\left[\frac{\partial U_i}{\partial x_j}+\frac{\partial U_j}{\partial x_i}\right],$$

wherein U is the mean velocity based on the Reynolds average, K is the turbulence kinetic energy, and ν_T is the eddy viscosity which is isotropic. Such a representation of turbulence is often not effective from both theoretical and phenomenological points of view, and the shortcomings associated with it are fully discussed by Speziale [1]. To over come some of these, models that are nonlinear (i.e., quadratic) in the mean strain rate were proposed in the form of a constitutive relation [3,4]. Speziale [3] employed tensor and dimensional analyses, together with invariance constraints, to derive his model. Yoshizawa's model [4] was obtained by appealing to a two-scale direct-interaction approximation. The application of these models depend on the empirical evaluation of the model constants. Apart from the specific values of the constants, these two models have quite similar structure, and both were able to predict anisotropy in Reynolds stresses in a noncircular duct problem.

The present study addresses the need for a more effective approach in the development of two-equation turbulence models, and in this context the renormalization-group (RNG)-theory-based models are examined for further development. While the application of renormalization-group theory to turbulence has at-

tracted much attention [5–18], it is important to realize that these calculations fall into two distinct categories: (a) ϵ-RNG [5–9], pioneered by Forster, Nelson, and Stephen [14], and (b) recursion RNG [10–13] (denoted from now on as r-RNG) pioneered by Rose [15]. These techniques have been critiqued [6,16–18] and compared [12]. Here we wish to point out that in the ϵ-RNG, a small parameter ϵ is introduced into the exponent of the forcing correlation function (with the forcing function being introduced into the momentum equation). The theory is then developed for $\epsilon \ll 1$, and all constants generated are evaluated in this limit $\epsilon \ll 1$. However, at the same time, all exponents that are ϵ dependent are evaluated at $\epsilon = 4$ [17]. In fact, $\epsilon = 4$ is required in the ϵ-RNG to recover the Kolmogorov energy spectrum in the inertial range [17]. This not only plays some havoc with the evaluation of constants, it also leads to a closure problem: RNG-induced interactions that can be shown to be irrelevant in the limit $\epsilon \ll 1$ can in no way now be shown to be irrelevant in the limit $\epsilon \to 4$. Yet in ϵ-RNG theories (which require $\epsilon \to 4$) these higher-order nonlinearities are *assumed* to be unimportant [6,12,16]. Moreover, ϵ-RNG theory can only take into account nonlocal interactions [6,10,16]. However, the procedure is quite amenable and Rubinstein and Barton [7] have derived a Reynolds stress model using ϵ-RNG methods that is qualitatively similar to that of Speziale [3] and Yoshizawa [4].

On the other hand, r-RNG does not rely on an ϵ expansion, and treats explicitly the cubic nonlinearities induced into the renormalized momentum equation. Moreover, r-RNG can handle both local and nonlocal interactions. Effects such as the cusp behavior in the transport coefficients as $k \to k_c$ are recovered in these theories (here k_c is the cutoff wave number separating the large scale from the local resolvable scales) [13,19–24]. These effects are the consequences of local interactions and the cubic nonlinearities introduced by the RNG procedure. However, one of the major difficulties to the application of r-RNG for turbulent flows governed by the Navier-Stokes equation was that the eddy viscosity was determined as a fixed point of a very complicated integrodifference equation. This drawback has now been removed by extending the theory to handle the iterative removal of infinitesimal wave-number bands [25]. Now, as in ϵ-RNG, the eddy viscosity is readily determined from the solution of a relatively simple differential equation. Unlike ϵ-RNG, however, the transport coefficients are determined over the whole resolvable scales and not just in the wave-number limit $k \to 0$.

In the present work, the r-RNG procedures are used to evaluate the local interaction contributions to the Reynolds stresses in a formal manner. We have compared the predictions of the long-wavelength, nonlocal interaction limit of ϵ-RNG with the corresponding nonlocal interaction limit of r-RNG for several transport coefficients [the eddy viscosity and the Prandtl number]. In this nonlocal limit, the results from ϵ-RNG and r-RNG were nearly identical. We thus expect this similarity to hold in the nonlocal interaction contribution to the Reynolds stresses, and here concentrate on determining the r-RNG local interaction contribution to τ_{ij}. It is shown that the r-RNG-based model introduces two additional terms arising from the local interaction effects that are of higher order than those obtained using the ϵ-RNG method by considering only the long-wave length, nonlocal interaction limit. The first of these two terms as well as those from the conventional turbulence models are shown to be a part of the integrity basis used in the representation of the anisotropic part of the Reynolds stress tensor [26–28]. The second term, which arises from pressure-strain coupling, is a higher-order dispersive term, and cannot be represented within this integrity basis.

This Reynolds stress model is then applied for turbulent flow past a backward-facing step which has played a central role in benchmarking the performance of turbulence models for separated flows. During the past decade—beginning with Ref. [29]—various two-equation turbulence models have been tested and compared with the experimental data of Kim, Kline, and Johnston [30] and Eaton and Johnston [31] for the backstep problem. Initial results [29] indicated that the standard K-ε model, with wall functions, underpredicted the reattachment point by a substantial amount on the order of 20–25 %. Several independent studies have been subsequently published using alternative forms of the K-ε model wherein a variety of conflicting results have been reported. Considering the need to predict accurately separated turbulent flows—which can have a wealth of important scientific and engineering applications—the proposed model is applied to the backstep problem. The computations based on a sufficiently resolved finite-volume algorithm show that the proposed model based on the recursive application of the renormalization-group theory (developed independently without any *ad hoc* empiricism) can yield a prediction for the reattachment point that is within a few percent of the experimental result. The r-RNG model performance is also compared with that of the standard two-equation K-ε model and the ϵ-RNG model for this backstep problem. The physical implications of these results will be also discussed in detail in the sections to follow.

II. FORMULATION OF THE PHYSICAL PROBLEM

The turbulent motion of viscous, incompressible fluids are governed by the Navier-Stokes equations, which may be analyzed using classical single-point closure based on Reynolds decomposition of all physical variables. The resulting averaged equations of motions are of the form

$$\frac{\partial U_i}{\partial t} + U_\alpha \frac{\partial U_i}{\partial x_\alpha} = -\frac{\partial P}{\partial x_i} + \nu_0 \frac{\partial^2 U_i}{\partial x_\alpha \partial x_\alpha} + \frac{\partial \tau_{i\alpha}}{\partial x_\alpha} , \quad (1)$$

$$\frac{\partial U_\alpha}{\partial x_\alpha} = 0 , \quad (2)$$

where U_i is the mean velocity, P is the mean pressure, ν_0 is the kinematic viscosity of the fluid, and τ_{ij} is the Reynolds stress tensor. While the physical aspects of turbulent flows are best described by the above equations, limitations in computer capacity and speed preclude their direct solution for complex flows of engineering impor-

tance. The current practice for high Reynolds number flows of engineering interest therefore involves some type of modeling for Reynolds stresses. The commonly used turbulence models are based on the calculation of one-point first and second moments such as the mean velocity, mean pressure, and turbulent kinetic energy.

In the present work we consider the development of Reynolds stress model by the r-RNG formulation and its application. In this context it is convenient to express the equations of motion using the Fourier representation:

$$\left[\frac{\partial}{\partial t}+\nu_0 k^2\right]u_i(\mathbf{k},t) = M_{i\alpha\beta}(k)\int d^3p\, u_\alpha(\mathbf{p},t)u_\beta(\mathbf{k}-\mathbf{p},t)\ , \quad (3)$$

$$k_\alpha u_\alpha(\mathbf{k},t)=0\ . \quad (4)$$

It is important to note here that *no* random forcing is introduced, unlike in the ϵ-RNG theories where it plays a critical role in introducing the small parameter ϵ. The nonlinear coupling coefficient

$$M_{i\alpha\beta}(k)=\frac{1}{2\hat{i}}[k_\beta D_{i\alpha}(k)+k_\alpha D_{i\beta}(k)]\ , \quad (5)$$

where $\hat{i}=\sqrt{-1}$, and $D_{\alpha\beta}$ is the projection operator defined by

$$D_{\alpha\beta}(k)=\delta_{\alpha\beta}-\frac{k_\alpha k_\beta}{k^2}\ . \quad (6)$$

A scale factor h is now introduced to partition the wave-number space to N bands, such that

$$k_c=k_N=h^N k_0\ ,$$
$$k_{N-1}=h^{N-1}k_0,\ldots,k_1=hk_0\ , \quad (7)$$
$$k_0=O(k_d)\ ,$$

where k_c is the cutoff wave number that separates the large scale from the small scale, and k_d is of the order of the Kolmogorov dissipation wave number. The velocity field is then decomposed in the Fourier space such that $u_i=u_i^>\theta(k-k_h)+u_i^<\theta(k_h-k)$ [wherein θ is the Heaviside unit step function, $k_h(h=1,N)$ is the local cutoff wave number, the superscript $<$ represents large resolvable scale quantities, and $>$ represents small unresolved scales with respect to the local cutoff wave number]. The evolution of these components can be directly obtained from (3) as

$$\left[\frac{\partial}{\partial t}+\nu_0 k^2\right]u_i^>(\mathbf{k},t)=M_{i\alpha\beta}(k)\int d^3p[u_\alpha^<(\mathbf{p},t)u_\beta^<(\mathbf{k}-\mathbf{p},t)+2u_\alpha^>(\mathbf{p},t)u_\beta^<(\mathbf{k}-\mathbf{p},t)+u_\alpha^>(\mathbf{p},t)u_\beta^>(\mathbf{k}-\mathbf{p},t)]\ , \quad (8)$$

$$\left[\frac{\partial}{\partial t}+\nu_0 k^2\right]u_i^<(\mathbf{k},t)=M_{i\alpha\beta}(k)\int d^3p[u_\alpha^<(\mathbf{p},t)u_\beta^<(\mathbf{k}-\mathbf{p},t)+2u_\alpha^>(\mathbf{p},t)u_\beta^<(\mathbf{k}-\mathbf{p},t)+u_\alpha^>(\mathbf{p},t)u_\beta^>(\mathbf{k}-\mathbf{p},t)]\ . \quad (9)$$

It should be noted that in the ϵ-RNG approach one is forced into taking the large-scale infrared limit $k\to 0$. In essence, this forces a spectral gap between the resolvable part of the flow field and the small unresolved scales. If this spectral gap were somehow present initially, it would be quickly populated in just a few eddy turnover times. Thus retaining only the distant interactions may not be appropriate. In fact, it has been shown [13] that the energy-transfer function that corresponds to local interactions accounts for most of the energy flow out of the resolvable scales. It thus seems important to retain both local and nonlocal interactions in the modeling of the Reynolds stress, and this can be readily achieved by r-RNG. In particular, it is apparent that the Reynolds stress $\tau_{ij}=\tau_{ij}^{>>}+\tau_{ij}^{><}$ has two components. The $\tau_{ij}^{>>}$ part arises from the infrared limit of $k\to 0$ and is due to the $u_i^>$-$u_i^>$ distant interaction limit, while the $\tau_{ij}^{><}$ part arises from the $0<k\le k_c$ spectrum and is due to the $u_i^>$-$u_i^<$ local interaction limit. Thus in the ϵ-RNG model of Rubinstein and Barton [7], the Reynolds stress $\tau_{ij}=\tau_{ij}^{>>}$ and is obtained purely from the $u_i^>$-$u_i^>$ interaction in the small unresolved scale momentum equation (8).

We now consider the contribution to the Reynolds stress that arises from the local interaction:

$$\tau_{ij}^{><}=-\int d^3p[u_i^<(\mathbf{k}-\mathbf{p})u_j^>(\mathbf{p})+u_j^<(\mathbf{k}-\mathbf{p})u_i^>(\mathbf{p})]\ . \quad (10)$$

Herein $\mathbf{u}^<(\mathbf{k}-\mathbf{p})$ corresponds to the Fourier-transformed velocity field in the resolvable large scales, $|\mathbf{k}-\mathbf{p}|<k_1$, while $\mathbf{u}^>(\mathbf{p})$ corresponds to the small-scale field with $|\mathbf{p}|>k_1$, and k_1 is the wave number which separates the resolvable from the small unresolved scales.

Some care is needed in the evaluation of local interaction $\tau_{ij}^{><}$. In particular, it is important to preserve certain properties that $\tau_{ij}^{><}$ must satisfy (a) $\tau_{ij}^{><}\to 0$ as the turbulent kinetic energy $K\to 0$, and (b) $\tau_{ij}^{><}$ is Galilean invariant. Constraint (a) arises from Eq. (10): in the limit of turbulent kinetic energy $K\to 0$, the subgrid scale velocity field $\mathbf{u}^>\to 0$, hence $\tau_{ij}^{><}\to 0$. Constraint (b), while being physically obvious, has been shown to be rigorously satisfied by r-RNG in that the cubic nonlinearities, which are an essential element of the renormalized Navier-Stokes equation, do not destroy the Galilean invariance [25]. Now if one follows blindly the usual r-RNG procedures [10–13], then in the elimination of the first subgrid shell one would substitute the subgrid velocity field of solution of Eq. (9):

$$u_i^>(\mathbf{p})=\frac{M_{i\alpha\beta}(p)}{\nu_0 p^2}\int d^3j\, u_\alpha^<(\mathbf{j})u_\beta^<(\mathbf{j}-\mathbf{p})+\cdots \quad (11)$$

into Eq. (10), where $\cdots$ refers to terms that will not contribute to $\tau_{ij}^{><}$. Implicit in the substitution of (11) is the assumption that the turbulent kinetic energy K is

nonzero. However, in the limit of $K \to 0$, this substitution is inappropriate since the right-hand side of (11) is nonzero while $\mathbf{u}^> \to 0$. To overcome this problem and the somewhat more subtle loss of Galilean invariance, we introduce the factor $(p-k)_\alpha(p-s)_\alpha/k_c^2$ into the integrand on the right-hand side of (10), and integrate over s for $\tau_{ij}^{><}$. This factor ensures that constraints (a) and (b) are indeed enforced, since $k_c = O(\varepsilon/K^{3/2}) \to \infty$ as $K \to 0$. Indeed, following Yakhot and Orszag [5], this cutoff wave number k_c can be related to the turbulent kinetic energy K by

$$K = \int_{k_c}^{\infty} E(p)dp = \tfrac{3}{2} C_K \frac{\varepsilon^{2/3}}{k_c^{2/3}} \tag{12}$$

on using the Kolmogorov inertial range spectrum for $E(p)$, and where C_K is the Kolmogorov constant. Thus, the cutoff wave number k_c which separates the resolvable scales by the subgrid scales is given by

$$k_c = \frac{\varepsilon}{K^{3/2}} (\tfrac{3}{2} C_K)^{3/2} . \tag{13}$$

Hence after the elimination of the first spectral subgrid band, Eq. (10) becomes

$$\tau_{ij}^{><}(\mathbf{k})|_1 = -\frac{1}{k_c^2} \left[\int d^3p\, d^3s \frac{(p_\alpha - k_\alpha)(p_\alpha - s_\alpha)}{\nu_0 p^2} \times M_{j\gamma\delta}(p) u_\gamma^<(s) u_\delta^<(p-s) \times u_i^<(k-p) + (i \leftrightarrow j) \right] , \tag{14}$$

where p is in the subgrid region, while the arguments of all the velocity fields are in the resolvable scales. The second term in (14) is obtained by $i \leftrightarrow j$ interchange in the first term. After the removal of the second subgrid shell,

$$\tau_{ij}^{><}(\mathbf{k})|_2 = \tau_{ij}^{><}(\mathbf{k})|_1 - \int d^3p [u_i^<(\mathbf{k}-\mathbf{p}) u_j^>(\mathbf{p}) + u_j^<(\mathbf{k}-\mathbf{p}) u_i^>(\mathbf{p})] , \tag{15}$$

where $k < k_2$. For $k_2 < k < k_1$, the subgrid velocity field is obtained by standard RNG procedures, with molecular viscosity ν_0 replaced by the renormalized eddy viscosity ν_1:

$$u_i^>(\mathbf{p}) = \frac{M_{i\alpha\beta}(p)}{\nu_1(p) p^2} \int d^3j\, u_\alpha^<(\mathbf{j}) u_\beta^<(\mathbf{j}-\mathbf{p}) + \cdots . \tag{16}$$

Hence the local interaction Reynolds stress, after the elimination of the first two subgrid shells, is given by

$$\tau_{ij}^{><}(\mathbf{k}) = -\frac{1}{k_c^2} \sum_{h=1}^{2} \left[\int d^3p\, d^3s \frac{(p_\alpha - k_\alpha)(p_\alpha - s_\alpha)}{\nu_k(p) p^2} \times M_{j\gamma\delta}(p) u_\gamma^<(s) u_0^<(p-s) \times u_i^<(k-p) + (i \leftrightarrow j) \right] . \tag{17}$$

After the elimination of the Nth subgrid spectral band, the local interaction Reynolds stress becomes

$$\tau_{ij}^{><}(\mathbf{k}) = -\frac{1}{k_c^2} \sum_{h=1}^{N} \left[\int d^3p\, d^3s \frac{(p_\alpha - k_\alpha)(p_\alpha - s_\alpha)}{\nu_h(p) p^2} \times M_{j\gamma\delta}(p) u_\gamma^<(s) u_\delta^<(p-s) \times u_i^<(k-p) + (i \leftrightarrow j) \right] . \tag{18}$$

In (18) summation is over all the spectral bands eliminated, and $\nu_h(p)$ is the renormalized eddy viscosity [10–13]. We now proceed to the differential limit of infinitesimal spectral shells, so that [15]

$$\sum_h \frac{1}{\nu_h(p)} \to \frac{1}{\nu(k_c)} \left[\frac{p}{k_c} \right]^{4/3} \tag{19}$$

for the Kolmogorov $k^{-5/3}$ inertial range energy spectrum. With

$$M_{j\gamma\delta}(p) = \frac{1}{2\hat{i}} \left[\delta_{j\gamma} p_\delta + \delta_{j\delta} p_\gamma - 2 \frac{p_j p_\gamma p_\delta}{p^2} \right] , \tag{20}$$

(18), in the differential limit for infinitesimal spectral subgrid shells, becomes

$$\tau_{ij}^{><}(\mathbf{k}) = -\frac{1}{2\hat{i}\nu(k_c) k_c^{10/3}} \left[\int d^3p\, d^3s \frac{(p_\alpha - k_\alpha)(p_\alpha - s_\alpha)}{p^{2/3}} \times \left\{ p_\beta u_j^<(s) u_\beta^<(p-s) u_i^<(k-p) + p_\beta u_\beta^<(s) u_j^<(p-s) u_i^<(k-p) - 2\frac{p_\beta p_j p_\gamma}{p^2} u_\beta^<(s) u_\gamma^<(p-s) u_i^<(k-p) \right\} + (i \leftrightarrow j) \right] . \tag{21}$$

On taking the inverse Fourier transforms of (21), we obtain the contribution from local interactions in physical space to the Reynolds stress:

$$\tau_{ij}^{><}(\mathbf{x}) = \frac{1}{(2\pi)^3 \nu(k_c) k_c^{10/3}} \left[\frac{\partial U_i(\mathbf{x})}{\partial x_\alpha} \int d^3x' \left\{ g_1(\mathbf{x}-\mathbf{x}') \frac{\partial U_j(\mathbf{x}')}{\partial x'_\beta} \frac{\partial U_\beta(\mathbf{x}')}{\partial x'_\alpha} + g_2(\mathbf{x}-\mathbf{x}') \frac{\partial}{\partial x'_j} \left[\frac{\partial U_\gamma(\mathbf{x}')}{\partial x'_\beta} \frac{\partial^2 U_\beta(\mathbf{x}')}{\partial x'_\alpha \partial x'_\gamma} \right] \right\} + (i \leftrightarrow j) \right] . \tag{22}$$

In (22) we have identified the reasonable velocity field in the physical space with the mean velocity U_i, and the nonlocal kernels $g_1(\mathbf{x}-\mathbf{x}')$ and $g_2(\mathbf{x}-\mathbf{x}')$ are defined by

$$g_1(\mathbf{r})=\int \frac{\exp(\hat{i}\mathbf{p}\cdot\mathbf{r})}{p^{2/3}}d^3p,\quad g_2(\mathbf{r})=\int \frac{\exp(\hat{i}\mathbf{p}\cdot\mathbf{r})}{p^{8/3}}d^3p\ . \tag{23}$$

The structure of these nonlocal kernels is dependent on the cutoff wave number k_c. Indeed,

$$g_1(r)=\frac{4\pi}{r}\int_{k_c}^{2k_c} p^{1/3}\sin(pr)dp$$
$$=\frac{4\pi}{r}k_c^{4/3}\int_1^2 p'^{1/3}\sin(k_c p' r)dp'\ , \tag{24}$$

$$g_2(r)=\frac{4\pi}{r}k_c^{-2/3}\int_1^2 p'^{-5/3}\sin(k_c p' r)dp'\ , \tag{25}$$

where the integration limits are obtained from the partial average [15] over the nearest unresolved band. These integral kernels will reduce the local expressions in the limit of $k_c \gg 1$. Noting that $\sin(k_c x)/x \to \pi\delta(x)$ as $k_c \to \infty$, we see that, for $k_c \gg 1$,

$$g_1(r)/4\pi \approx 3.58 k_c^{4/3}\delta(r)\ ,$$
$$g_2(r)/4\pi \approx 1.74 k_c^{-2/3}\delta(r)\ . \tag{26}$$

Hence, using this local approximation of the kernels (strictly valid only in the limit of $k_c \gg 1$), the r-RNG evaluation of $\tau_{ij}^{><}(\mathbf{x})$ in (22) reduces to the simple algebraic form

$$\tau_{ij}^{><}(\mathbf{x})=C_{R1}\frac{K^4}{\varepsilon^3}\left[\frac{\partial U_i}{\partial x_\alpha}\frac{\partial U_j}{\partial x_\beta}\frac{\partial U_\beta}{\partial x_\alpha}+i\leftrightarrow j\right]$$
$$+C_{R2}\frac{K^7}{\varepsilon^5}\left[\frac{\partial U_i}{\partial x_\alpha}\frac{\partial}{\partial x_j}\left[\frac{\partial U_\beta}{\partial x_\gamma}\frac{\partial^2 U_\gamma}{\partial x_\alpha \partial x_\beta}\right]+(i\leftrightarrow j)\right], \tag{27}$$

where use has been made of Kraichnan's [32] result

$$\nu(k_c)k_c^{4/3}=0.19C_K^2\varepsilon^{1/3}\ . \tag{28}$$

Now for most turbulent flows of interest, the cutoff wave number k_c in (13) will vary considerably throughout the flow domain. In order to have a tractable model for $\tau_{ij}^{><}(\mathbf{x})$, we wish to enforce the local approximation for the kernels g_1 and g_2 so as to obtain an algebraic form for the Reynolds stress $\tau_{ij}^{><}(\mathbf{x})$, while still treating flows with finite k_c. Clearly, the coefficients C_{R1} and C_{R2} will be complicated functions of the flow quantities. In particular, C_{R1} and C_{R2} may be expressed as

$$C_{R1}=C_{R2}(\varepsilon,K,\eta,\zeta)\ \text{ and }\ C_{R2}=C_{R2}(\varepsilon,K,\eta,\zeta)\ , \tag{29}$$

where the strain rate $\eta\equiv(S_{\alpha\beta}S_{\alpha\beta})^{1/2}$, with $S_{\alpha\beta}\equiv\frac{1}{2}[(\partial U_\alpha/\partial x_\beta)+(\partial U_\beta/\partial x_\alpha)]$, and the rotation rate $\zeta\equiv(W_{\alpha\beta}W_{\alpha\beta})^{1/2}$, with $W_{\alpha\beta}\equiv\frac{1}{2}[(\partial U_\alpha/\partial x_\beta)-(\partial U_\beta/\partial x_\alpha)]$.

The nonlocal contribution to the Reynolds stress, $\tau_{ij}^{>>}(\mathbf{x})$, is the somewhat standard [3,4,7]. From a RNG perspective and based on earlier comparisons [12,13,25] between the nonlocal ϵ-RNG and the $k\to 0$ of the r-RNG results, it seems appropriate here to use Rubinstein and Barton's [7] ϵ-RNG evaluation of the (nonlocal) Reynolds stress:

$$\tau_{ij}^{>>}=-\tfrac{2}{3}K\delta_{ij}+\nu_T\left[\frac{\partial U_i}{\partial x_j}+\frac{\partial U_j}{\partial x_i}\right]$$
$$-\frac{K^3}{\varepsilon^2}\left[C_{\tau1}\left[\frac{\partial U_i}{\partial x_\alpha}\frac{\partial U_j}{\partial x_\alpha}\right]^*+C_{\tau2}\left[\frac{\partial U_i}{\partial x_\alpha}\frac{\partial U_\alpha}{\partial x_j}+\frac{\partial U_j}{\partial x_\alpha}\frac{\partial U_\alpha}{\partial x_i}\right]^*+C_{\tau3}\left[\frac{\partial U_\alpha}{\partial x_i}\frac{\partial U_\alpha}{\partial x_j}\right]^*\right], \tag{30}$$

as a negligible difference is expected from the $k\to 0$ of the r-RNG analysis. We thus will use the coefficients as derived by Rubinstein and Barton [7] $C_{\tau1}=0.034$, $C_{\tau2}=0.104$, and $C_{\tau3}=-0.014$, and $(\ )^*$ denotes the deviatory part of the expression within the parentheses. The first two terms correspond to the linear model, with the isotropic eddy viscosity $\nu_T=C_\mu K^2/\varepsilon$, where ε is the turbulence dissipation. Canonically, the value of $C_\mu\approx 0.09$ is based on empirical data from equilibrium boundary layer flows. The third term in (30) is the main result of Rubinstein and Barton [7], is quadratic in mean strain rate, and includes the effect of convection and diffusion. It has the same structure as other second-order models but with somewhat different coefficients [3,4].

Hence our final model for the Reynolds stress, including both the nonlocal and local interactions, is obtained by combining Eqs. (27)–(30):

$$\tau_{ij}=-\tfrac{2}{3}K\delta_{ij}+\nu_T\left[\frac{\partial U_i}{\partial x_j}+\frac{\partial U_j}{\partial x_i}\right]-\frac{K^3}{\epsilon^2}\left[C_{\tau1}\left[\frac{\partial U_i}{\partial x_\alpha}\frac{\partial U_j}{\partial x_\alpha}\right]^*+C_{\tau2}\left[\frac{\partial U_i}{\partial x_\alpha}\frac{\partial U_\alpha}{\partial x_j}+\frac{\partial U_j}{\partial x_\alpha}\frac{\partial U_\alpha}{\partial x_i}\right]^*+C_{\tau3}\left[\frac{\partial U_\alpha}{\partial x_i}\frac{\partial U_\alpha}{\partial x_j}\right]^*\right]$$
$$+C_{R1}\frac{K^4}{\varepsilon^3}\left[\frac{\partial U_i}{\partial x_\alpha}\frac{\partial U_j}{\partial x_\beta}\frac{\partial U_\beta}{\partial x_\alpha}+i\leftrightarrow j\right]+C_{R2}\frac{K^7}{\varepsilon^5}\left[\frac{\partial U_i}{\partial x_\alpha}\frac{\partial}{\partial x_j}\left[\frac{\partial U_\beta}{\partial x_\gamma}\frac{\partial^2 U_\gamma}{\partial x_\alpha\partial x_\beta}\right]+(i\leftrightarrow j)\right]. \tag{31}$$

The last two terms are those that we have calculated from r-RNG. It is of some interest to recast the above expression for the Reynolds stress obtained from the r-RNG model into an integrity basis representation, such as is commonly employed for the anisotropic part of the Reynolds stress tensor $b_{ij}=(\tau_{ij}-\frac{2}{3}K\delta_{ij})/2K$, in the following form-invariant manner [26–28]:

$$b_{ij}=\sum_{\lambda} G^{(\lambda)}T_{ij}^{(\lambda)} , \tag{32}$$

where $T_{ij}^{(\lambda)}$ is the integrity basis for functions of symmetric and antisymmetric tensors, and the coefficients $G^{(\lambda)}$ are scalar functions of the irreducible invariants of the strain rate tensor S_{ij} and the rotation rate tensor W_{ij} [26–28]:

$$\begin{aligned}
T_{ij}^{(1)}&=S_{ij} ,\\
T_{ij}^{(2)}&=S_{i\alpha}W_{\alpha j}-W_{i\alpha}S_{\alpha j} ,\\
T_{ij}^{(3)}&=S_{i\alpha}S_{\alpha j}-\tfrac{1}{3}S_{\alpha\alpha}\delta_{ij} ,\\
T_{ij}^{(4)}&=W_{i\alpha}W_{\alpha j}-\tfrac{1}{3}W_{\alpha\alpha}\delta_{ij} ,\\
T_{ij}^{(5)}&=W_{i\alpha}S_{\alpha\beta}S_{\beta j}-S_{i\alpha}S_{\alpha\beta}W_{\beta j} ,\\
T_{ij}^{(6)}&=W_{i\alpha}W_{\alpha\beta}S_{\beta j}+S_{i\alpha}W_{\alpha\beta}W_{\beta j}\\
&\quad-\tfrac{2}{3}(S_{\alpha\beta}W_{\beta\gamma}W_{\gamma\alpha})\delta_{\alpha\beta} ,\\
T_{ij}^{(7)}&=W_{i\alpha}S_{\alpha\beta}W_{\beta\gamma}W_{\gamma j}-W_{i\alpha}W_{\alpha\beta}S_{\beta\gamma}W_{\gamma j} ,\\
T_{ij}^{(8)}&=S_{i\alpha}W_{\alpha\beta}S_{\beta\gamma}S_{\gamma j}-S_{i\alpha}S_{\alpha\beta}W_{\beta\gamma}S_{\gamma j} ,\\
T_{ij}^{(9)}&=W_{i\alpha}W_{\alpha\beta}S_{\beta\gamma}S_{\gamma j}+S_{i\alpha}S_{\alpha\beta}W_{\beta\gamma}W_{\gamma j}\\
&\quad-\tfrac{2}{3}(S_{\alpha\beta}S_{\beta\gamma}W_{\gamma\varepsilon}W_{\varepsilon\alpha})\delta_{ij} ,\\
T_{ij}^{(10)}&=W_{i\alpha}S_{\alpha\beta}S_{\beta\gamma}W_{\gamma\varepsilon}W_{\varepsilon j}-W_{i\alpha}W_{\alpha\beta}S_{\beta\gamma}S_{\gamma\varepsilon}W_{\varepsilon j} .
\end{aligned} \tag{33}$$

Recently, Gatski and Speziale [28] have applied this integrity basis to determine an explicit algebraic stress model for three-dimensional turbulent flows based on a systematic derivation from a hierarchy of second-order closure models. In their applications, they have restricted themselves to a model [28] which involves just the tensors $T_{ij}^{(1)}$, $T_{ij}^{(2)}$, and $T_{ij}^{(3)}$. It can readily be shown that the $k=0$ part of the Reynolds stress, $\tau_{ij}^{>>}$, specified in (30), involves the tensors $T_{ij}^{(1)}$, $T_{ij}^{(2)}$, $T_{ij}^{(3)}$, and $T_{ij}^{(4)}$ from the integrity basis given by (33). The $\tau_{ij}^{>>}$ part of the Reynolds stress is common to both ϵ-RNG and r-RNG. However, unlike ϵ-RNG, there is now a finite-k spectral contribution $\tau_{ij}^{><}$ to the Reynolds stress in r-RNG. It can be shown that the first term in (27) involves the tensors $T_{ij}^{(5)}$ and $T_{ij}^{(6)}$ of the integrity basis (33). The second term in (27), on the other hand, cannot be expressed in this second-order basis because of the intrinsic higher-order derivatives involved. This term is a direct consequence of the r-RNG formulation, and contributes to the dispersive effects of the Reynolds stress.

III. TURBULENT FLOW PAST A BACKWARD-FACING STEP—A CASE STUDY

The problem to be considered is the fully developed turbulent flow of an incompressible viscous fluid past a backward-facing step (a schematic is provided in Fig. 1). Calculations will be conducted for an expansion ratio (outlet channel height: inlet channel height) E of 3:2 and the Reynolds number $\mathrm{Re}=132\,000$ based on the inlet centerline mean velocity and outlet channel height (which corresponds to that of Kim, Kline, and Johnston [30] and Eaton and Johnston [31]).

The governing equations used to describe the separated flow past the backward-facing step consists of the time-averaged equations of motion (1) and (2), along with the Reynolds stress specified by (31). Closure is achieved by specifying turbulent kinetic energy K and dissipation ε—quantities that are directly related to the length and time scales—through the development of transport equations. In this work, we do not attempt to derive these equations from r-RNG (this is a very major undertaking, and beyond the scope of this paper) but rather utilize the standard two-equation turbulence model of the following form that is considered widely in the literature [1]:

$$\frac{\partial K}{\partial t}+U_j\frac{\partial K}{\partial x_j}=\mathcal{P}-\varepsilon+\frac{\partial}{\partial x_i}\left[\left(\nu_0+\frac{\nu_T}{\alpha_K}\right)\frac{\partial K}{\partial x_i}\right] , \tag{34}$$

$$\begin{aligned}
&\frac{\partial \varepsilon}{\partial t}+U_j\frac{\partial \varepsilon}{\partial x_j}\\
&\quad=C_{\varepsilon 1}\frac{\varepsilon}{K}\mathcal{P}-C_{\varepsilon 2}\frac{\varepsilon^2}{K}+\frac{\partial}{\partial x_i}\left[\left(\nu_0+\frac{\nu_T}{\alpha_\varepsilon}\right)\frac{\partial \varepsilon}{\partial x_i}\right]-\mathcal{R} ,
\end{aligned} \tag{35}$$

where $\nu=\nu_0+\nu_T$ is the total viscosity,

$$\mathcal{P}=\tau_{ij}\left(\frac{\partial U_i}{\partial x_j}\right) \tag{36}$$

is the turbulence production, and

$$\mathcal{R}=2\nu_0 S_{ij}\overline{\left(\frac{\partial u_j}{\partial x_i}\frac{\partial u_i}{\partial x_j}\right)} \tag{37}$$

is the turbulent strain rate correlation term. The quantities $C_{\varepsilon 1}$, $C_{\varepsilon 2}$, α_K, and α_ε are dimensionless and treated as constants that are model dependent. A major problem with this type of closure is the treatment of the strain rate correlation $\mathcal{R}$. No theory exists, at present, that can

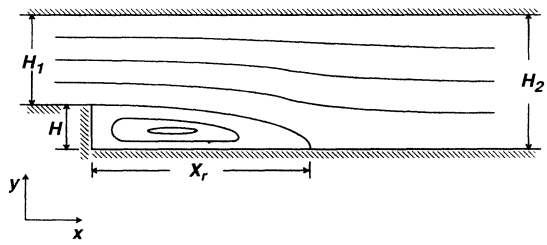

FIG. 1. Physical configuration and coordinate system.

treat this term from first principles. A somewhat successful modeling of this term has been achieved by Yakhot *et al.* [9] for shear flows, but various *ad hoc* procedures had to be invoked—procedures totally independent of ϵ-RNG procedures. In attempting to assess the importance of the local interaction contribution to the Reynolds stress $\tau_{ij}^{><}$ on separated flows, it was felt that one should avoid encumbering the results with these *ad hoc* procedures. Hence, as is customary in the standard K-ε model, we have also neglected this strain rate correlation term $\mathcal{R}$. To maintain some form of consistency, the standard K-ε model values for the constants

$$C_{\varepsilon 1}=1.44,\quad C_{\varepsilon 2}=1.92,\quad \alpha_K=1.0,\quad \alpha_\varepsilon=1.3\ , \tag{38}$$

rather than those values determined by the other theories, are used. The above equations are solved subject to the following boundary conditions [33].

(a) Inlet profiles for U, K, and ε are specified five step heights upstream of the step corner (U is taken from the experimental data [30,31], and the corresponding profiles for K and ε are computed from the model formulated for channel flow).

(b) The law of the wall is used at the upper and the lower walls.

(c) Conservative extrapolated outflow conditions are applied 30 step heights downstream of the step corner. These conditions involve the following: (i) the V component of the velocity for the cells at the outflow boundary are obtained by extrapolation; (ii) the U component of the velocity is then computed by the application of a mass balance; and (iii) the scalar quantities such as pressure, turbulent kinetic energy, and turbulent dissipation are all obtained by extrapolation. It was found that a downstream channel length of about 30 step heights was needed to ensure that the local error for all the quantities was of the same order as the interior values.

A finite volume method which relies on solving the discretized equations by a line relaxation method with the repeated application of the tridiagonal matrix solution algorithm is modified and applied for the present case to obtain the steady state solution [33,34]. The computed solution was assumed to have converged to its steady state when the root-mean-square of the average difference between successive iterations was less than 10^{-4} for the mass source [34]. Approximately 2000 iterations were needed for the convergence of the standard K-ε model; this corresponds to approximately 20 min of CPU time in a partially vectorized mode on the Cray-YMP supercomputer using 64-bit precision. The r-RNG-based K-ε model requires approximately 33% more CPU time due to the fact that the additional terms in the RNG-based K-ε model have to be evaluated during each iteration. These correction terms are dispersive—an additional feature that slows convergence.

The issue of resolution is crucial for the backstep problem, and calculations indicate that a 200×100 mesh yields a fully grid-independent solution [33]. All the computations conducted in this study were performed using this 200×100 nonuniform mesh. As indicated earlier, the inlet conditions were specified five step heights upstream of the step corner, and the outlet boundary conditions were specified 30 step heights downstream of the step corner. It is crucial that a sufficient distance downstream of the reattachment period be allowed before the outflow conditions are imposed. Many earlier computations of the backstep problem were in significant error due to the imposition of fully developed outflow conditions too close to the reattachment point. Furthermore, it is crucial that a fine mesh be used near the step corner for computational accuracy. It should also be noted that the law of the wall does not formally apply to separated turbulent boundary layers. However, since the separation point is fixed at the corner of the backstep—and the

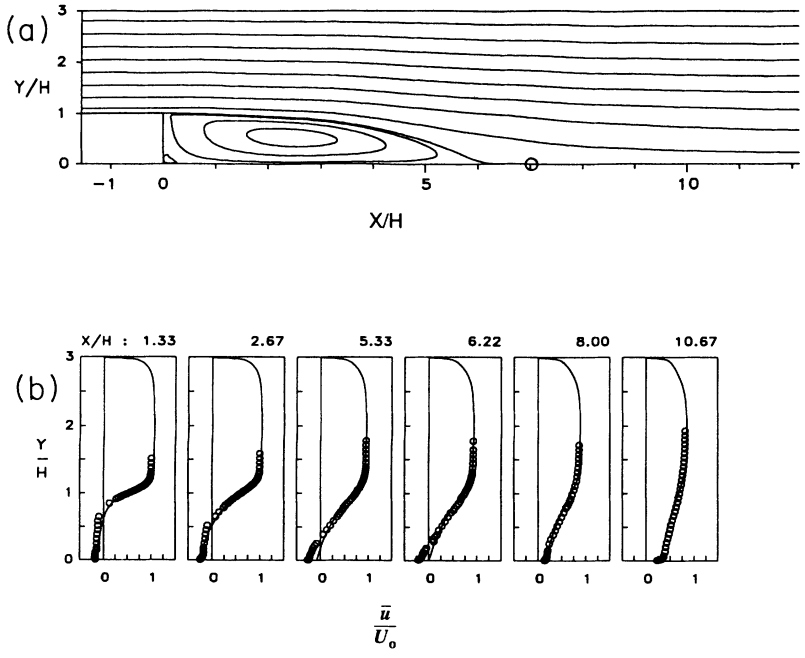

FIG. 2. Computed flow field with the standard K-ε model ($E=3{:}2$; $\mathrm{Re}=132\,000$; 200×100 mesh; $C_\mu=0.09$; $C_{\varepsilon 1}=1.44$; $C_{\varepsilon 2}=1.92$; $\sigma_K=1.0$; $\sigma_\varepsilon=1.3$; and $\kappa=0.41$). (a) Contours of mean streamlines. (b) Mean velocity profiles at selected locations (——, computed solutions; ○, experiments of Kim, Kline, and Johnston [30] and Eaton and Johnston [31]).

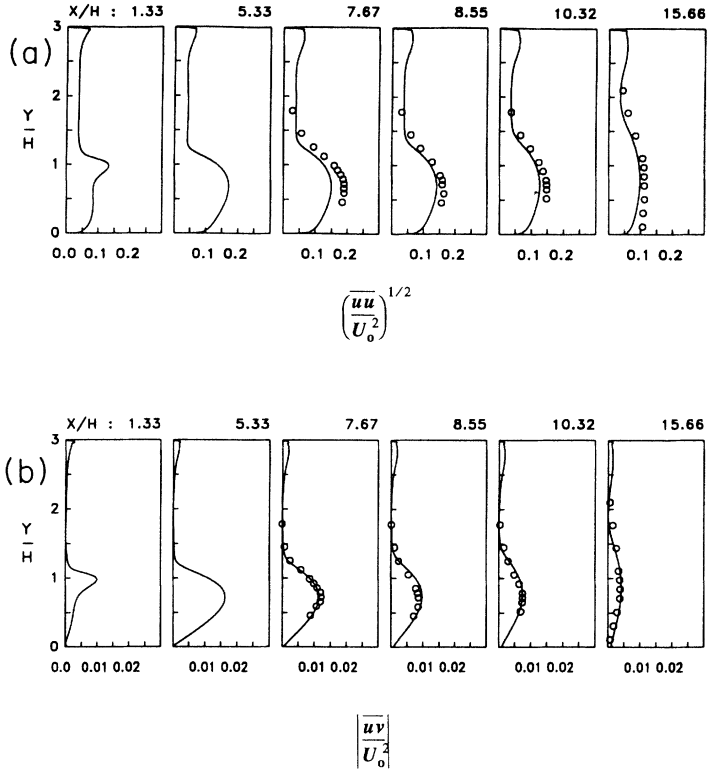

FIG. 3. Computer turbulence stresses with the standard K-ε model ($E=3{:}2$; Re=132 000; 200×100 mesh; $C_\mu=0.09$; $C_{\varepsilon 1}=1.44$; $C_{\varepsilon 2}=1.92$; $\sigma_K=1.0$; $\sigma_\varepsilon=1.3$; $\kappa=0.41$; ——, computed solutions; and ○, experiments of Kim, Kline, and Johnston [30] and Eaton and Johnson [31]). (a) Turbulence intensity profiles. (b) Turbulence shear stress profiles.

flowfield is solved iteratively so that the friction velocity u_τ can be updated until it converges—major errors do not appear to result from its use [33].

First, results will be presented for the standard K-ε model. For this case—as well as the other results to follow—computed results for the mean velocity streamlines, the streamwise mean velocity profiles, the streamwise turbulence intensity profiles, and the turbulence shear stress profiles are compared with the Kim, Kline, and Johnson [30] experimental data as updated by Eaton and Johnston [31]. In Fig. 2(a) the computed streamlines are shown, indicating reattachment at $X_r/H\approx 6.1$—a result which is approximately 15% underprediction of the experimental reattachment point of $X_r/H\approx 7.1$. In this context, it is noted that due to the very nature of the flow field—turbulent separated flow characterized by a massive recirculation region straddled by a sharp shear layer—unsteadiness of both temporal and spatial kinds have been observed and documented [30,31]. The spatial uncertainties are known to include variations in the reattachment point along the spanwise and the axial directions [31,35]. Thus a conservative estimate of 7.1 ± 0.5 for this geometry, where the value of 7.1 represents the time-averaged mean value along the midspan of the channel, is generally accepted. The experimental data for the mean velocity field and the turbulence quantities utilized in this text for comparison with the computational results corresponds to the time-averaged mean along the midspan of the channel.

In Fig. 2(b), the streamwise mean velocity profiles predicted by the standard K-ε model are compared with the experimental data. Except in the vicinity of the reattachment point, the comparisons are fairly good. More serious discrepancies between the model predictions and the experimental data occur in the initial part of the recovery zone for the streamwise turbulence intensity profiles, as shown in Fig. 3(a). However, the model predictions for the turbulence shear stress profiles are reasonably good, as can be seen from Fig. 3(b).

Next we consider computations based on the aniso-

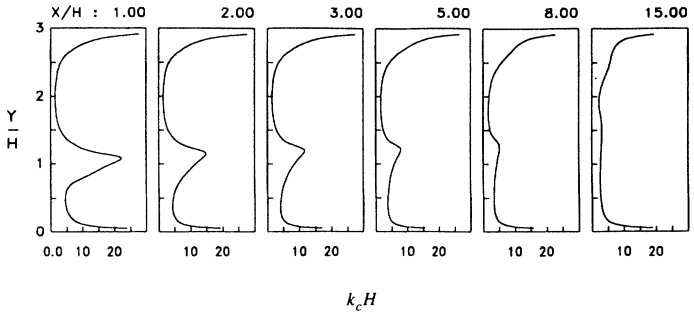

FIG. 4. Variation of cutoff wave number k_cH at several locations downstream of the step for the recursion RNG K-ε model ($E=3{:}2$; Re=132 000; 200×100 mesh; ——, computations; ○, experiments of Kim, Kline, and Johnston, 1980 [30] and Eaton and Johnston, 1981 [31]).

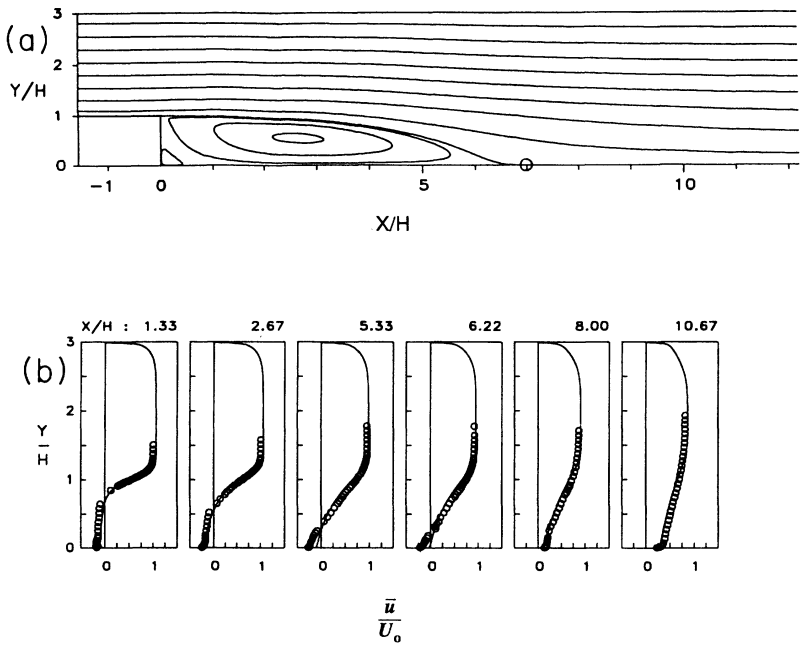

FIG. 5. Computed flow field with the recursion RNG K-ε model based on a finite cutoff wave number [$E=3{:}2$; Re$=132\,000$; 200×100 mesh; $C_\mu=0.09$; $C_{\varepsilon1}=1.44$; $C_{\varepsilon2}=1.92$; $\sigma_K=1.0$; $\sigma_\varepsilon=1.3$; $\kappa=0.41$; $C_{R1}=-25.0\times10^{-3}$; and $C_{R2}=-0.0352\times10^{-3}$]. (a) Contours of mean streamlines. (b) Mean velocity profiles at selected locations (——, computed solutions; ○, experiments of Kim, Kline, and Johnston [30] and Eaton and Johnston [31]).

tropic Reynolds stress formulation of the r-RNG model. For computational efficiency, the radial parts of the nonlocal kernels g_1 and g_2 are approximated by one-dimensional δ functions. This is a good approximation if $k_c \gg 1$. In Fig. 4, the variation of k_c (normalized by the step height and expressed as k_cH) with y/H is shown at various locations downstream of the step, x/H. As can be seen, the magnitude of k_c is at least an order of magnitude larger than the grid size employed ($k_cH>1$ for the 200×100 mesh used). Thus the local representation of g_1 and g_2, for the backstep problem, seems a good approximation. Unfortunately, the angular dependence of these coefficients on the mean strain rate and the mean rotational rate is not so easily approximated, with explicit functional dependence on these rates leading to difficult numerical computations. As a first attempt at assessing the importance of local interaction effects on the Reynolds stress, $\tau_{ij}^{><}$, the coefficients are approximated as constants. Based on the recent success of Yakhot *et al.* [9] in invoking functional *Ansätze* that certain coefficients could have when the strain rate correlation $\mathcal{R}$ was modeled, we expect that ignoring the functional forms of

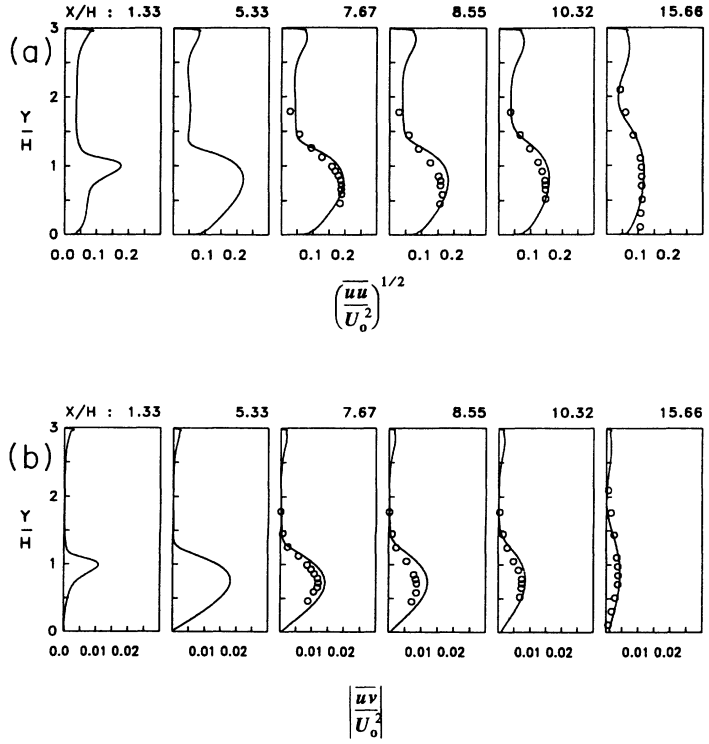

FIG. 6. Computed turbulence stresses with the recursion RNG K-ε model based on a finite cutoff wave number ($E=3{:}2$; Re$=132\,000$; 200×100 mesh; $C_\mu=0.09$; $C_{\varepsilon1}=1.44$; $C_{\varepsilon2}=1.92$; $\sigma_K=1.0$; $\sigma_\varepsilon=1.3$; $\kappa=0.41$; $C_{R1}=25.0\times10^{-3}$; $C_{R2}=0.0352\times10^{-3}$; ——, computed solutions; and ○, experiments of Kim, Kline, and Johnson [30] and Eaton and Johnston [31]). (a) Turbulence intensity profiles. (b) Turbulence shear stress profiles.

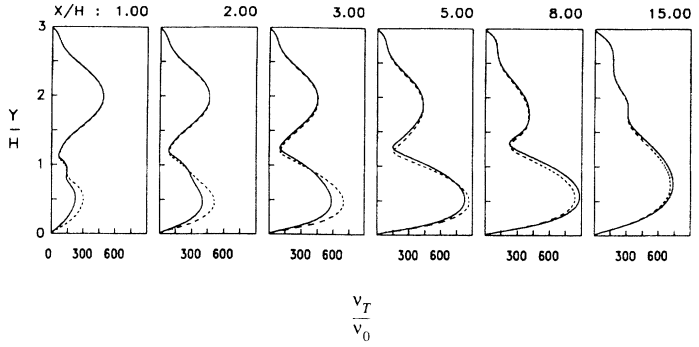

FIG. 7. Variation of the eddy viscosity ν_T/ν_0 at several locations downstream of the step (— — —, standard K-ε model; ——, recursion RNG K-ε model). $E=3{:}2$, $\mathrm{Re}=132\,000$, 200×100 mesh.

C_{R1} and C_{R2} will underestimate the robustness and accuracy of the Reynolds stresses. Nevertheless, it is deemed more appropriate here to apply the theory without adding on these extraneous functional *Ansätze*. It is also evident that the angular dependences of $g_2(|\mathbf{x}-\mathbf{x}'|)$ are much stronger than those for $g_1(|\mathbf{x}-\mathbf{x}'|)$; the second term in (22) is much stronger than that of the first term in (22). This is because of the higher-order derivatives present. Moreover, these angular integrations are also dependent on the spatial position due to the changing flow characteristics. A simple mean-value-type approximation is applied to estimate these angular integrations, and for the present analysis we find,

$$C_{R1}=0.025,\quad C_{R2}=0.342\times10^{-3}\,. \tag{39}$$

Now it will be demonstrated that use of the proposed r-RNG-based Reynolds stress model can yield a more significant improvement in the results. The computed streamlines for the flow field shown in Fig. 5(a) have a mean reattachment point $X_r/H\approx6.72$, a result which is about 5% lower than the experimental value. The corresponding mean velocity profiles shown in Fig. 5(b) indicate very good agreement with the experimental results. It should be noted that computations performed based on the ε-RNG-based model for the same flow conditions and model constants yield a mean reattachment point $X_r/H\approx6.42$ (not shown herein). The difference in the size of the separated flow region can be clearly attributed to the contributions from the Reynolds stress terms representing the local interactions effects in the r-RNG model. In particular, it is found that around 80% of this improvement comes from the C_{R1} term.

Furthermore the overall agreement between the turbulence intensity and the shear stresses with the experimental data shown in Figs. 6(a) and 6(b) are also good. The most notable difference between the predictions of the RNG-based Reynolds stress models and the standard K-ε model lies in the streamwise turbulence [Fig. 6(a)]. The slight trough-shaped variation predicted in this region is consistent with more recent independent experiments [35].

In addition, to illustrate the differences associated with the modeling of the Reynolds stresses, the variation of the turbulent eddy viscosity normalized with respect to its molecular counterpart, ν_T/ν_0, is shown at several locations downstream of the backward-facing step in Fig. 7. As can be seen in the recirculation region, the eddy viscosity predicted by the standard K-ε model is generally larger than that due to the r-RNG, leading to substantial reduction in the size of the separated flow region [cf. Figs. 2(a) and 5(a)].

The wall pressure coefficient is an important parameter for engineering applications. In Figs. 8(a) and 8(b), the pressure coefficients C_p $(=2[p-p_r]/U_r^2$, where p_r and U_r are the reference pressure and velocity, which are tak-

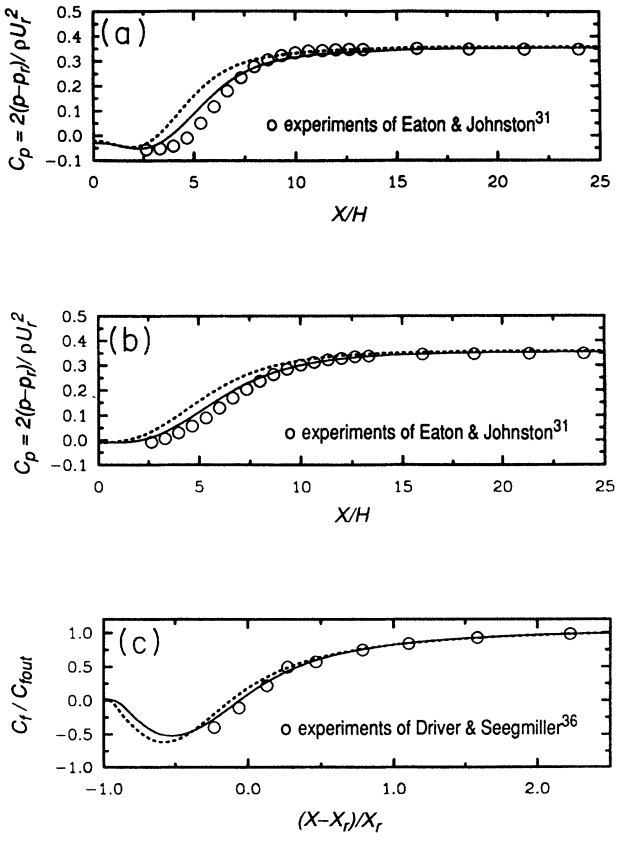

FIG. 8. Comparison of the predicted wall distributions with experiments [— — —, standard K-ε model; ——, recursion RNK K-ε model] $E=3{:}2$; $\mathrm{Re}=132\,000$. (a) Pressure coefficient along the bottom wall (○, experiments of Eaton and Johnston [31]). (b) Pressure coefficient along the top wall (○, experiments of Eaton and Johnston [31]). (c) Skin friction coefficient along the bottom wall (○, scaled experimental data of Driver and Seegmiller [36]).

en at the centerline of the inlet) obtained from the standard K-ε model and the RNG-based Reynolds stress model at the top and bottom walls are compared with the experimental data of Eaton and Johnson [31]. As can be seen, both the standard K-ε model and the RNG-based Reynolds stress model perform comparably well in reproducing the experimental trends. The skin friction coefficients $C_f = 2u_\tau^2/U_r^2$ obtained from the standard K-ε model and the r-RNG Reynolds stress model are compared with the scaled experimental data of Driver and Seegmiller [36] for the bottom wall in Fig. 8(c). Here we make use of the fact that the ratio $C_f/C_{f\infty}$, when taken as a function of the normalized distance $(X-X_r)/X_r$, is independent of the expansion ratio (given that $C_{f\infty}$ is the fully developed skin friction coefficient and X_r is the reattachment point). As can be seen, the r-RNG-based Reynolds stress model performs better; however, both models are probably within the uncertainty of the experimental data.

Finally, in Table I a comparison of the reattachment points for the two-equation turbulence models considered herein is given. To illustrate the improvements due to the inclusion of the higher-order terms arising from the r-RNG formulation of the Reynolds stress, the results for the standard two-equation model that is linear in strain rate is shown first, and is followed by three different quadratic models—a model that is derived by the renormalization-group theory solely by considering the nonlocal effects (Rubinstein and Barton [7]), a model wherein the effects of turbulence are represented similar to non-Newtonian fluids involving a quadratic and frame-indifferent relation between stress and strain rate (Speziale [3]), as well as a model that is derived by a general perturbation method based on two-scale direct interaction approximation [4,37,38]. As can be seen, the inclusion of the second-order terms in strain rate leads to an improvement of about 6.5% (with the ϵ-RNG model [7] yielding about 5.2%, while the general perturbation method based model [4,37,38] shows an improvement of about 6.5%). However, it should be noted that, unlike the ϵ-RNG model, in the other quadratic models the values of the coefficients ($C_{\tau 1}$, $C_{\tau 2}$, and $C_{\tau 3}$) are empirically obtained by calibration (Speziale [3] uses channel flow data, while the coefficients attributed to Yoshizawa's model [4] were obtained after calibration based on flows in noncircular ducts [37,38]. In this context, it is interesting to note that the reattachment point is rather insensitive to the specific values of these coefficients. The results from the r-RNG model are shown next, and, as can be seen, the importance of local interaction effects in the modeling of Reynolds stresses is quite evident—about 5% improvement (over that of Rubinstein and Barton [7], wherein only the nonlocal effects are considered) in the prediction of reattachment point and the mean flow field in the separated flow region. While similar improvements are possible by other means, the present improvements are effected by a systematic analysis based on the renormalization-group theory approach, without the use of *ad hoc* empiricism.

IV. CONCLUSIONS

The recursion renormalization-group (r-RNG) theory is utilized to develop a local interaction contribution to the Reynolds stresses for the prediction of turbulent separated flows. Unlike the small-parameter ϵ-RNG theories, which can only treat the interaction of the long-wavelength modes, r-RNG theories incorporate both local and nonlocal interactions of all relevant resolvable scales. A formal evaluation of the Reynolds stress

TABLE I. Turbulent flow past a backward-facing step—reattachment length for different two-equation models. All models utilize the standard form of the transport equations for the turbulence kinetic energy, and dissipation with the following model coefficients: $C_\mu = 0.09$, $C_{\varepsilon 1} = 1.44$, $C_{\varepsilon 2} = 1.92$, $\alpha_\varepsilon = 1.0$, and $\alpha_\varepsilon = 1.3$. The strain rate correlation $\mathcal{R}$ is not included. Mean experimental reattachment point $X_r/H \approx 7.1$ [31].

Model	X_r/H	Reynolds stress model
Standard K-ε model	6.10	Isotropic with $\tau_{ij} = -\frac{2}{3}K\delta_{ij} + \nu_T(\partial_j U_i + \partial_i U_j)$
ε-RNG model [7]	6.42	Anisotropic with quadratic effects $\tau_{ij} = \tau_{ij}^{>>}$[a]
Nonlinear K-ϵ model [3]	6.46	Anisotropic with quadratic effects in τ_{ij}[b]
TSDIA model [4]	6.49	Anisotropic with quadratic effects in τ_{ij}[c]
r-RNG model (present)	6.72	Anisotropic with cubic effects: $\tau_{ij} = \tau_{ij}^{>>} + \tau_{ij}^{><}$[d]

[a]From Eq. (30) based on ϵ-RNG model [7] ($C_{\tau 1} = 0.034$, $C_{\tau 2} = 0.104$, and $C_{\tau 3} = -0.014$).

[b]Based on the model proposed by Speziale [3], wherein effects of turbulence are represented similar to non-Newtonian fluids using a quadratic relationship between stress and strain rates ($C_{\tau 1} = 0.041$, $C_{\tau 2} = 0.014$, and $C_{\tau 3} = -0.014$).

[c]Based on the general perturbation model of Yoshizawa [4] using the two-scale direct interaction approximation (TSDIA) with the coefficients obtained by calibration with turbulent flow in square ducts [37,38] ($C_{\tau 1} = 0.057$, $C_{\tau 2} = -0.167$, and $C_{\tau 3} = -0.0067$).

[d]From Eq. (31). If other formulations such as those of Speziale or Yoshizawa are used for $\tau_{ij}^{>>}$, the coefficients $C_{\tau 1}$, $C_{\tau 2}$, and $C_{\tau 3}$ will be correspondingly altered, and minor improvements noticed in terms of an increase in the reattachment length. For example, with the model proposed by Speziale[b] the reattachment length $X_r/H \approx 6.77$, when local effects arising from r-RNG are now included.

by the r-RNG is presented. Of particular importance is the appearance of two new terms in $\tau_{ij}^{><}$ due to local interactions. The nonlocal interaction term is expected to be essentially the same as that derived by Rubinstein and Barton [7] in their ϵ-RNG treatment of $\tau_{ij}^{>>}$. This correspondence between the ϵ-RNG results and the nonlocal ($k \rightarrow 0$ limit) r-RNG results has already been noted in earlier works [12,13,25].

The effects of these local interaction terms in τ_{ij} is examined by considering turbulent flow past a backward-facing step as a test case. For numerical convenience, the functional dependence of the new r-RNG generated coefficients C_{R1} and C_{R2} on the strain rate and rotation rate—while expected to be of considerable importance [9]—is not treated here. Instead, simple approximations are utilized to reduce these coefficients to constants. Because of the simplification, the testing of our model here can be seen as an underestimate of the robustness of this formulation. The detailed numerical results presented here demonstratc that the proposed r-RNG model can yield very good predictions for the turbulent flow of an incompressible viscous fluid over a backward-facing step.

It should be remembered that the deficiencies of two-equation models as well established, particularly in turbulent flows with body forces or Reynolds stress relaxation effects [1]. Consequently, the findings of this study should not be interpreted as an unequivocal endorsement of two-equation RNG models. Nonetheless, this study shows that properly calibrated two-equation turbulence models, which account for the anisotropy of the turbulent stresses, can be effective for the prediction of turbulent separated flows. Future work will consider more sophisticated evaluation of the functional forms of the coefficients C_{R1} and C_{R2} as well as the development of r-RNG-based transport equations for the turbulent kinetic energy and dissipation.

ACKNOWLEDGMENTS

The authors are indebted to Dr. T. B. Gatski and Dr. M. Y. Hussaini for their helpful comments and encouragement during the course of this work. This research was supported by the National Aeronautics and Space Administration under NASA Contract No. NAS1-19480, while the authors were in residence at the Institute for Computer Applications in Science and Engineering (ICASE), NASA Langley Research Center, Hampton, VA 23681. One of the authors (G.V.) was also partially supported by the Department of Energy.

[1] C. G. Speziale, Ann. Rev. Fluid Mech. **23**, 107 (1991).
[2] B. E. Launder and D. B. Spalding, Comput. Methods Appl. Mech. Eng. **3**, 269 (1974).
[3] C. G. Speziale, J. Fluid Mech. **178**, 459 (1987).
[4] A. Yoshizawa, Phys. Fluids **27**, 1377 (1984).
[5] V. Yakhot and S. A. Orszag, J. Sci. Comput. **1**, 3 (1986).
[6] L. M. Smith and W. C. Reynolds, Phys. Fluids A **4**, 364 (1992).
[7] R. Rubinstein and J. M. Barton, Phys. Fluids A **2**, 1472 (1990).
[8] V. Yakhot and L. M. Smith, J. Sci. Comput. **7**, 35 (1992).
[9] V. Yakhot, S. A. Orszag, S. Thangam, T. B. Gatski, and C. G. Speziale, Phys. Fluids A **4**, 1510 (1992).
[10] Y. Zhou, G. Vahala, and M. Hossain, Phys. Rev. A **37**, 2590 (1988).
[11] Y. Zhou, G. Vahala, and M. Hossain, Phys. Rev. A **40**, 5865 (1989).
[12] Y. Zhou and G. Vahala, Phys. Rev. A **46**, 1136 (1992).
[13] Y. Zhou and G. Vahala, Phys. Rev. E **47**, 2503 (1993).
[14] D. Forster, D. Nelson, and M. Stephen, Phys. Rev. A **16**, 732 (1977).
[15] H. A. Rose, J. Fluid Mech. **81**, 719 (1977).
[16] R. H. Kraichnan, Phys. Fluids **30**, 2400 (1987).
[17] S. H. Lam, Phys. Fluids A **4**, 1007 (1992).
[18] W. D. McComb, *The Physics of Fluid Turbulence* (Clarendon, Oxford, 1990).
[19] R. H. Kraichnan, J. Atmos. Sci. **33**, 1521 (1976).
[20] D. C. Leslie and G. L. Quarini, J. Fluid Mech. **91**, 65 (1979).
[21] J. P. Chollet and M. Lesieur, J. Atmos. Sci. **38**, 2747 (1981).
[22] J. A. Domaradzski, R. W. Metcalfe, R. S. Rogallo, and J. J. Riley, Phys. Rev. Lett. **58**, 547 (1987).
[23] M. Lesieur and R. Rogallo, Phys. Fluids A **1**, 718 (1989).
[24] J. R. Chasnov, Phys. Fluids A **3**, 188 (1991).
[25] Y. Zhou and G. Vahala, Phys. Rev. E **47**, 2503 (1993); also available as NASA-ICASE Report No. 93-1 (1993) (unpublished).
[26] A. J. M. Spencer, in *Continuum Physics,* edited by A. C. Eringen (Academic, New York, 1971), Vol. 1, p. 1.
[27] S. B. Pope, J. Fluid Mech. **72**, 331 (1975).
[28] T. B. Gatski and C. G. Speziale, NASA-ICASE Report 92-58; J. Fluid Mech. **254**, 59 (1993).
[29] *Proceedings of the 1980-81 AFOSR-HTTM Stanford Conference on Complex Turbulent Flows,* edited by S. J. Kline, B. J. Cantwell, and G. M. Lilley (Stanford University Press, Stanford, CA, 1981).
[30] J. Kim, S. J. Kline, and J. P. Johnston, ASME J. Fluids Eng. **102**, 302 (1980).
[31] J. Eaton and J. P. Johnston, Technical Report MD-39, Stanford University, CA (1980) (unpublished).
[32] R. H. Kraichnan, J. Fluid Mech. **47**, 525 (1971).
[33] S. Thangam and C. G. Sepziale, AIAA J. **30**, 1314 (1992).
[34] D. G. Lilley and D. L. Rhode, NASA Contractor Report CF-3442 (1982) (unpublished).
[35] S. O. Kjelgaard, Master of Science Thesis, George Washington University, 1991 (unpublished).
[36] D. M. Driver and H. L. Seegmiller, AIAA J. **23**, 163 (1985).
[37] Y. Shimomura and A. Yoshizawa, J. Phys. Soc. Jpn. **55**, 1904 (1986).
[38] S. Nisizima, Trans. Jpn. Soc. Mech. Eng. **55B**, 991 (1989).